Title
Surface composition effects in electrocatalysis: Kinetics of oxygen reduction on well-defined Pt{sub 3}Ni and Pt{sub 3}Co alloy surfaces

Journal
Journal of Physical Chemistry B, 106(46)

Author
Ross, P.N.

Publication Date
2002-05-01

LBNL-50229

Surface Composition Effects in Electrocatalysis: Kinetics of Oxygen Reduction on Well-Defined Pt_3Ni and Pt_3Co Alloy Surfaces

V. Stamenković*, T.J. Schmidt, N.M. Marković and P.N. Ross

Materials Sciences Division, Lawrence Berkeley National Laboratory
University of California at Berkeley, CA 94720, USA

Abstract

The oxygen reduction reaction (ORR) has been studied on polycrystalline Pt_3Ni and Pt_3Co alloys in acid electrolytes using the rotating ring disk electrode (RRDE) method. Preparation and characterization of alloy surfaces were performed in ultra high vacuum (UHV). Clearly defined surface composition was determined via low energy ion scattering (LEIS) spectroscopy. Polycrystalline bulk alloys of Pt_3Ni and Pt_3Co were prepared in UHV having two different surface composition: one with 75 % Pt and the other with 100 % Pt. The latter we call a "Pt-skin" structure and is produced by an exchange of Pt and Co in the first two layers. The base voltammetry in 0.1 M $HClO_4$ solution of the 75% Pt alloy surface indicated a decrease of H_{upd} pseudocapacitance (ca. 30-40 $\mu C/cm^2$) consistent with the surface composition determined in UHV. With the exception of the "Pt-skin" surface on Pt_3Ni, all the alloy electrodes exhibited stable i-E curves with repeated cycling between 0.05-1.0 V at all temperatures. Activities of Pt-alloys for the ORR were compared to the polycrystalline Pt in 0.5M H_2SO_4 and 0.1M $HClO_4$ electrolytes in the temperature range of $293 < T < 333$ K. It was found that the order of activity is dependent on the nature of anions of supporting electrolytes: in H_2SO_4 the activity increased in the order $Pt_3Ni > Pt_3Co > Pt$; in $HClO_4$, however, the order of activities at 333 K was "Pt-skin"> $Pt_3Co > Pt_3Ni > Pt$. The catalytic enhancement was greater in 0.1 M $HClO_4$ than in 0.5 M H_2SO_4, with the maximum enhancement observed for the "Pt-skin" on Pt_3Co in 0.1 M $HClO_4$ being 3-4 times that for pure Pt. Catalytic enhancement of the ORR on Pt_3Ni and Pt_3Co vs. Pt was attributed to the inhibition of Pt-OH_{ad} formation *on* Pt sites surrounded by "oxide" covered Ni and Co atoms beyond 0.8 V. Kinetic analyses of RRDE data revealed that kinetic parameters for the ORR and the production of H_2O_2 on the Pt_3Ni, Pt_3Co and "Pt-skin" alloys are the same as on pure Pt: reaction order, m=1, two identical Tafel slopes in $HClO_4$ and a single Tafel slope in H_2SO_4, apparent activation energy, ≈ 21-25 kJ/mol. The fact that essentially the same kinetic parameters are assessed from the analysis of experimental results for the ORR on all three surfaces implies that the reaction mechanism on Pt_3Ni and Pt_3Co alloy surfaces is the *same* as one proposed for pure Pt, *i.e.,* a "series" $4e^-$ reduction pathway.

Keywords: electrocatalysis, alloys, platinum nickel, platinum cobalt, oxygen reduction reaction, surface composition

*corresponding author: vrstamenkovic@lbl.gov

1. Introduction

In the last few years considerable progress has been made in understanding the electrocatalysis the ORR by using well characterized Pt and Pt-bimetallic surfaces [1]. To this end, variations of metal surface crystallography and/or electronic properties by intermixing two or more metals has often been employed to delineated very impotent electrocatalytic trends. For example, it was demonstrated that the kinetics of the ORR on Pt(hkl) vary with the crystal face in a different manner depending on the electrolyte, suggesting that dependence of surface geometry arises primarily due to structure sensitive adsorption of specifically adsorbing anions [1-5]. To probe the electronic effects, the ORR kinetics was investigated on thin metal films grown epitiaxially on foreign metal substrates [6;7]. Several investigations have been carried out to determine the role of alloying in the electrocatalytic activity of Pt for the ORR [8-16]. It is unclear, however, whether there is any alloy of Pt that is more active than Pt itself. With an exception of work by Toda et al. [15], most of the studies reporting improved activity have been done on supported catalysts, where the kinetic measurements themselves are subject to considerable uncertainty [16;17]. One of the difficulties in determining the effect of alloying components using supported catalysts is that the activity of supported catalysts can have a wide range of values depending on its microstructure and/or method of preparation. Since the alloyed Pt catalysts particles may not have either the same particle size or shape as the Pt catalysts to which they are compared, a simple comparison of activity normalized either by mass or surface area is insufficient to identify a true alloying effect. Furthermore, in order to get insight into the relationship between the surface composition and the catalytic activity it is very important to determine if the surface segregation takes place during the preparation of bimetallic surfaces, i.e. enrichment of one element at the surface relative to the bulk [1;18-21]. The details of segregation are still not completely understood, especially in the case of segregation on nanoparticles which may differ from that of their bulk analog [22;23]. This is not

surprising considering that nanoclasters represent a finite quantity of material, so there is no infinite source/sink of constitute atoms and hence material balance constrains become important. Clearly all of these complexities on high surface area bimetallic catalysts reinforces the need for using well-characterized materials to identify the fundamental mechanisms at work in the electrocatalysis of the ORR.

In this paper the intrinsic catalytic activity of Pt_3Ni and Pt_3Co alloy catalysts for the ORR are studied on UHV prepared (annealing/sputtering cycles) and characterized (AES and LEIS) alloys in acid electrolytes. Emphasis will be placed on description of alloy surface preparation and characterization procedure as well as on kinetic studies of the ORR. It will be demonstrated that the ability to make a controlled and well characterized arrangement of two elements in the electrode surface region is essential to interpreting the kinetic results.

2. Experimental

2.1. Surface preparation and characterization

The polycrystalline bulk Pt-Ni and Pt-Co alloy electrodes used in this studies were prepared by conventional metallurgy. Bulk composition ($x_{Ni(Co),b}$) was assessed via x-ray fluorescence spectroscopy ($x_{Ni(Co),b} \approx 0.75$); x-ray diffraction showed all specimens to be single-phase *fcc* solid solutions of Pt and Ni(Co) having the expected lattice constant for 75 % Pt [24]. Cleaning, modification and surface characterization procedure were performed in UHV system, under base pressure of $2 \cdot 10^{-10}$ Torr range, which is equipped with an angular-resolving double pass cylindrical mirror analyzer PHI-DPCMA Φ15-255GAR with an electron source at its center. UHV cleaning procedure were done by repeating of sputtering-annealing cycles with Ar^+ and oxygen until Auger electron spectroscopy (AES) indicated that perfectly clean (carbon and oxygen free) surface was produced. AES spectra were recorded in derivative mode using the 3 keV

electron beam energy, 3 eV_{p-p} modulation and –5 μA beam current in the range from 140 to 900 eV.

In order to produce a different surface composition, clean samples were either annealed at 1000K or mildly sputtered with 0.5 keV beam of Ar^+ ions. The surface composition of alloy samples were determined by low energy ion scattering (LEIS). A compilation of surfaces analyzed by LEIS has been made by Watson [25]. LEIS spectra were taken with He^+ and Ne^+ beam energy of 1 keV with sample current from 5 to 30 nA at residual He/Ne pressure of $2.5 \cdot 10^{-8}$ Torr. Scattering angle was 127°, and the incidence angle was 45°. A Φ04-303A differentially pumped ion gun was used to raster He^+ or Ne^+ ion beam over approximately 3 mm×3 mm area. Time of recording was 60 s/spectrum. The clean Pt reference sample was prepared in the same manner. i.e. conventional metallurgy and pre-treated in UHV in exact the same way, mild sputter cleaning and/or annealing.

2.2 Electrochemical measurements

The UHV prepared and characterized alloy surfaces were withdrawn form the UHV introductory port (back-field with argon) into air and covered immediately with a drop of triply pyro-distilled water, for details see [26]. The electrode were then mounted in a rotating ring disk electrode and finally immersed in electrolyte under potential control at ~0.05V vs RHE in 0.5M H_2SO_4 (Baker, Ultrex) and 0.1M $HClO_4$ (Baker, Ultrex). Electrolytes were prepared with triple pyro-distilled water and thermostated at 293, 303, 313 and 333°K, by circulating constant temperature bath connected with water jacket of a standard three compartment electrochemical cell. The reference electrode was a saturated calomel electrode (SCE) separated by a bridge from the reference compartment. All potentials in this paper are, however, referenced to the reversible hydrogen electrode potential (RHE) at the same temperature (calibrated from hydrogen oxidation

reaction [27]) in the same electrolyte; argon, oxygen and hydrogen were bubbled through a glass frit (Air Products, 5N8 purity). During measuring the polarization curves for the ORR on the disk electrode the ring electrode was potentiostated at 1.15 V, a potential where peroxide oxidation reaction is under pure diffusion control; collection efficiency (N) for the ring-disk assembly is ca. 0.2. The geometrical surface area of the disk electrode was 0.283 cm^2, and all voltammograms were recorded with a sweep rate of either 50 of 20 mV/s.

3. Results and Discussion

3.1 Surface Composition

The relation between the surface and the bulk composition of alloys has been the subject of intensive research, in both theory and experiment [28-32]. For example, surface enrichment of Au is always detected for $Au_3Pd(100)$ [33], $Au_3Pd(110)$ [34] and $Cu_3Au(111)$ [35] alloy surfaces. According to UHV studies, $Pt_{78}Ni_{22}(111)$ [36], $Pt_{80}Co_{20}(001)$ [37] and $Pt_{80}Co_{20}(111)$ [38] alloys exhibits a highly structured compositional oscillations in the first three atomic layers. The studies revealed that for the (111) and (100) crystals the outermost layer of the clean, annealed surfaces are *pure* Pt, which we shall call hereafter the "skin" structure, with Pt depletion in the second layer. It has been found that at least some catalytic properties of the "Pt-skin" structures in UHV are different from the pure Pt surface [18;37]. This was attributed to the electronic effect of intermetallic bonding of the Ni(Co)-rich second layer with the top-most Pt atoms. As we demonstrate below, the "skin" structure with a characteristic catalytic activity can also be created on polycrystalline Pt_3Ni and Pt_3Co alloys.

The AES and LEIS spectra of Pt_3Ni and Pt_3Co polycrystalline samples, obtained after either mild sputtering or annealing of specimens, are shown in Figure 1 and 2. The AES reveal that after spattering/annealing cycles both alloy surfaces were clean, showing characteristic Pt

(158, 168, 189, 199, 237, 251, 390 eV) and Ni (716, 783, 848 eV) (Figure 1a) or Pt and Co (656, 716, 775 eV) (Figure 1a and 2a) peaks. Quantitative surface analysis of the Pt-Ni(Co) alloy with AES is quite complicated, requiring modeling of emission from several subsurface layers with dynamical scattering of the outgoing Auger electron. Because the contribution of Auger emission from the several atomic layers in the Pt_3-Ni(Co) alloy causes the Pt/Ni(Co) AES ratio to be much different than the ratio would be with emission only from the first layer, AES has only been used to verify the cleanliness of alloy surfaces. In contrast, the true surface composition of outermost atomic layer of the Pt_3-Ni(Co) alloy can be obtained by utilizing LEIS, as shown in Figures 1b and 2b. The scattering peaks of the Pt and Ni(Co) are calculated from the classical equation for elastic collisions [39]. The data, obtained by 1 keV Ne^+ beam, show that the first layer of a clean annealed Pt_3-Ni(Co) surface contains only Pt atoms, implying that the "Pt-skin" structure can also be created on a polycrystalline Pt_3Ni(Co) alloy. The LEIS spectra taken after mild sputtering unambiguously show that Ni(Co) are indeed present in the outermost layer of the clean sputtered surface. Using the elemental sensitivity factors of polycrystalline materials [40] surface composition is estimated to 75% of Pt and 25% of Ni/Co, equal to bulk concentration of Pt_3Co and Pt_3Ni alloys (denoted hereafter as Pt_3Ni and Pt_3Co). As mentioned above, both annealed and mildly sputtered specimens were transferred into the electrochemical cell for further electrochemical characterization.

3.2 Cyclic Voltammetry

The corresponding cyclic voltammograms of mildly sputtered Pt, Pt_3Ni, Pt_3Co and "Pt-skin" electrodes recorded immediately following transfer from UHV in argon purged 0.1 M $HClO_4$ and 0.5M H_2SO_4 at 293K are shown in Figure 1c and 2c. Voltammetry shows three characteristic potential regions: the hydrogen adsorption potential region (denoted hereafter as the underpotentially deposited hydrogen, H_{upd}, $0 < E$ 0.35V), in which H_{upd} adsorption/desorption is

accompanied by desorption/adsorption of anions of the supporting electrolyte, is followed first by the double layer potential region (ca. 0.4 < E 0.7 V) and then by the oxide formation potential region, E > ca.0.7 V. As shown in Figures 1c and 2c, both the H_{upd} features as well the oxide formation on Pt are strongly affected by the nature of anions, e.g. in contrast to relatively broad H_{upd} peaks in $HClO_4$, two sharp H_{upd} peaks are observed in H_2SO_4 and the surface coverage by oxide is reduced in the latter electrolyte. These experimental observations for pure Pt are not new and they are consistent with the recent theoretical calculations that for polyatomic oxyanions the Pt-anion strength of interaction is mostly determined by the different degree of backdonation to the empty levels of the anions, being more pronounced for Pt-HSO_4^- than for Pt-ClO_4^- interaction [41]. Figures 1c and 2c show that although voltammograms of the sputtered Pt_3Ni and Pt_3Co alloys are very similar with Pt, the charge under the peaks in the H_{upd} potential regions decreases from ca. 190 $\mu C/cm^2$ (geo) on Pt to ca.160 $\mu C/cm^2$ (geo) on Pt_3Ni and 150 $\mu C/cm^2$ (geo) on Pt_3Co alloys. Assuming that alloying with Ni(Co) does not affect the binding of H_{upd} to the Pt surface and that neither Ni nor Co are active sites for adsorption of hydrogen, the difference in the pseudocapacitance assessed in the H_{upd} potential region between Pt and Pt alloys may serve as an estimate of the number of Pt surface atoms in Pt_3Ni and Pt_3Co alloys. The difference of ca. -30 $\mu C/cm^2$ between Pt and Pt_3Ni and ca. -40$\mu C/cm^2$ between Pt and Pt_3Co corresponds to ≈70% - 80% of Pt surface atoms, which is very close to the bulk composition of 75 at% Pt determined in UHV. For the "Pt-skin", in the H_{upd} region voltammatry shows a Pt(111)-like shape [42], e.g. a broad H_{upd} peak with the pseudocapacitance under the peak of ca. 145 $\mu C/cm^2$ (geo). The amount of adsorbed H_{upd} is considerably attenuated (by about 45 $\mu C/cm^2$) on the "Pt-skin" versus clean Pt. These results appears to validate previous observation that the "Pt-skin" created on the Pt_3Co(hkl) single crystal surfaces has different adsorption properties from its bulk analog, e.g., a significant reduction (ca. 10 %) in the CO binding energy versus the pure Pt surface of the same orientation

[18;37]. As suggested by Bardi and Ross for the Pt_3Co(hkl)-CO system, the change in Pt-H_{upd} interaction on the "skin" surface can be attributed to an electronic effects of intermetallic bonding of the Co second layer with the top-most Pt atoms. A significant decrease in the H_{upd} pseudocapacitance , may suggest that rather strong lateral repulsion exist among the H_{upd} species on the "Pt-skin", as was proposed for the Pt(111)-H_{upd} system. A close inspection of Figure 2 indicates that on the Pt_3Ni and Pt_3Co alloys as well as on the "Pt-skin" electrode the onset of oxide formation shifts towards more positive potentials, suggesting that alloying with Ni(Co) effects a fundamental change in the way Pt atoms interact with H_2O and anions of supporting electrolytes.

It is important to note that the base voltammetry of all four electrodes recorded above room temperature (not shown) are very similar to those observed at 293 K. These results are in accordance with the previous observation that temperature (in the range of 293-333 K) has rather small effect on the voltammetric features of polycrystalline Pt and Pt single crystals in acid [27;43] and alkaline [44] solutions. It is also important to emphasis that, aside from the "Pt-skin" structure for the Pt_3Ni alloy, all voltammetric features shown in Figure 2 were reproduced in the subsequent scans. The base voltammetry remained stable even at elevated temperature ($293 < T < 333$ K), implying that during the duration of experiment (including the measurements of ORR kinetics) there is no corrosion/dissolution of alloying components. However, the voltammetry for the Pt-skin structure of the Pt_3Ni alloy was not stable to potential cycling in the region shown and for that reason we will not present the ORR kinetic results with that sample.

3.3 Oxygen Reduction Kinetics

For the purpose of demonstrating the methodology of probing the kinetic activity of Pt_3Ni and Pt_3Co alloys a representative set of polarization curves for the ORR on the spattered Pt_3Co alloy in 0.1 M$HClO_4$ at 298 K along with there kinetic analyses, presented in the form of the Tafel plot of mass-transport corrected currents (insert b) and the Levich-Kotecky plots (insert c), are

shown in Figure 3. Starting at 1.0 V and sweeping the disk potential negatively, the ORR is first under a mixed kinetic-diffusion control ($0.8 < E < 1.0$ V) and then at more negative potentials well defined diffusion limiting currents (i_D) are recorded between 0.7 and 0.2 V. Figure 3 also shows that in both potential regions the ring currents (I_R) are a small fraction of i_D, implying that the ORR proceeds almost entirely through a $4e^-$ reduction pathway. The appearance of the peroxide oxidation currents parallels the adsorption of hydrogen on Pt_3Co electrode ($E < 0.2$ V), reaching the maximum of ca. 20% at 0.075V. Quantitative representation of the peroxide production (current efficiency) was calculated from the equation 1 [45]:

$$x_{H_2O_2} = \frac{2\,I_R/N}{i_D + I_R/N} \qquad (1)$$

where N is collection efficiency of the ring-disk electrode. As mentioned above, in subsequent potential cycles both i_D and I_R remain the same, confirming that the surface composition of alloys remains the same during the ORR experiments.

Figure 3b shows the Tafel plot which is assessed from the potentiodynamic measurements. The curve was fitted with two single least-squares regression lines by drawing the tangent through the points of what appear to be continuous curve. The best fit corresponds to two Tafel slopes; ca. 74 mV/dec for $E < 0.86$ V and ca. 113 mV/dec for $E > 0.86$ V. As will be discussed in section 3.4.3, the transition in the Tafel slope appears to be related to the change in the nature of oxygen-containing species with potential, a transition that strongly affects the ORR [4;46-50]. Figure 3c shows the so called Levich-Kautecky plot, Eq.2,

$$\frac{1}{i} = \frac{1}{i_k} + \frac{1}{i_d} \qquad (2)$$

which for various potentials yields straight line with intercepts corresponding to the kinetic current, i_k. Notice that this intercept gives the order of absolute kinetic activity of the P_3Co surface

for the ORR. In addition, the slope of the straight lines, the so-called "B-factor", allows one to assess the number of electrons involved in the oxygen reduction reaction. The experimental value of ca. $4.28 \cdot 10^{-2}$ mA $rpm^{0.5}$ obtained from Figure 3c is in excellent agreement with the theoretical value of $4.27 \cdot 10^{-2}$ mA $rpm^{0.5}$, calculated for the four electron process from the Levich equation [51], using a literature data for oxygen solubility [52;53], c_0 ($c_0 = 1.26 \cdot 10^{-3}$ $molL^{-1}$), oxygen diffusivity [54], D ($D = 1.93 \cdot 10^{-5}$ cm^2s^{-1}), and kinematic viscosity of the electrolyte [52], ν ($\nu = 1.009 \cdot 10^{-2}$ cm^2s^{-1}). The linearity of the plots in Figure 3c implies a first-order dependence of O_2 kinetics on the Pt_3Co alloy (25% Co). Since the measurements of the kinetics as a function of partial pressure of O_2 are not available, the reaction order (m) was checked further from log i vs. $\log[i-i_d/i_d]$ functionality (not shown) using data from Figure 3c, for details see ref. [44]. The value of m=1.09 was obtained, confirming first order dependence of the kinetics of ORR on the Pt_3Co surface. All important kinetic parameters, obtained by using the same methodology as described above, for the ORR on Pt, sputtered Pt_3Ni(Co), and the "Pt-skin" Pt_3Co electrode in 0.1 M $HClO_4$ and 0.5 M H_2SO_4 at two temperatures are listed in Table 1.

Potentiodynamic polarization curves for 75% Pt alloy surfaces are shown for the ORR first in 0.1 M $HClO_4$ (Figure 4) and then in 0.5 M H_2SO_4 (Figure 5). Corresponding curves for pure Pt of Pt in both electrolytes are also shown as a reference. A close inspection of Figures 4 and 5 reveals that the reaction rates on Pt, Pt_3Ni and Pt_3Co are much higher in $HClO_4$ than in H_2SO_4. Furthermore, the order of activity is also dependent on the supporting electrolyte. For example, in $HClO_4$ Pt_3Co is more active than Pt_3Ni, while in H_2SO_4 Pt_3Ni is the most active electrode. The fact that activities are significantly higher in $HClO_4$ than in H_2SO_4, i.e. the same electrode is always less active in H_2SO_4 than in $HClO_4$, suggests that bisulfate adsorption on Pt sites inhibits the reduction by blocking the initial adsorption of O_2 [3], but it does not affect the reaction pathway, since no H_2O_2 is detected on the ring electrode in the kinetically controlled potential region.

Figures 4a and 5a show that H_2O_2 is also not detected during the ORR on Pt_3Co and Pt_3Ni electrodes in both electrolytes. In fact, in the potential region of $0.05 < E < 1$ V similarly small amounts of H_2O_2 are detected on the ring electrode on all three surfaces at 293 K, implying that, even though Pt_3Co and Pt_3Ni electrodes are more active than Pt, the reaction pathway of the ORR on Pt alloys may be the same as for a pure Pt electrode. At higher temperatures (Figures 4b and 5b) the polarization curves are qualitatively similar to the curves recorded at room temperature, having the same order of activity as at 293 K.

The results for the ORR on the "Pt-skin" electrode in 0.1 M $HClO_4$ are shown in Figure 6. Clearly, at 333 K the "Pt-skin" structure is more active than both pure Pt and 75 % Pt-25% Co alloy surface (insert of Figure 6), suggesting that an uniform monoatomic layer of Pt surface atoms, with Pt depletion and Co enrichment in the second layer, has unique catalytic properties. These results show that the kinetics of the ORR are dependent not only on the nature of alloying component ($Pt < Pt_3Ni < Pt_3Co$) but also on the exact arrangement of the alloying element in the surface region ($Pt_{bulk} < Pt_3Co <$ "Pt-skin" on Pt_3Co).

The effect of temperature on the rate of the ORR is clearly visible in Figures 4 and 5. As expected, the kinetics of the ORR is higher at elevated temperatures, reflecting the temperature dependence of the chemical rate constant which is approximately proportional to the $\exp(-\Delta H^{\#}/kT)$, where $\Delta H^{\#}$ is the apparent enthalpy of activation (here after simply termed as the activation energy) k is the Boltzman constant. The activation energies are evaluated at a fixed overpotential (η) using the Arrhenious equation

$$\left.\frac{\partial\left(\log i_k\right)}{\partial\left(1/T\right)}\right|_{\eta} = \frac{\Delta H^{*}}{2.3 \cdot R} \qquad (3)$$

The Arrhenius plots at η=0.3 V for three different catalysts are shown as an insert in Figure 4. The activation energies determined from the least square regressions are essentially identical and range between 20-23 kJ/mol, see Table 1. These values are in close agreement with values reported for single crystal platinum electrodes [55], polycrystalline platinum [56] and for carbon supported Pt [16] in both H_2SO_4 and $HClO_4$ solutions. In a previous study we reported activation energies between 20 and 25 kJ/mol for carbon supported Pt_3Ni and Pt_3Co alloys in a comparable potential range in $HClO_4$ [16]. One should keep in mind, however, that the assessments of activation energies at the same overpotential is only an estimate of the activation energy, i.e. $\Delta H^{\#}$ is the "apparent" activation energy. Kinetic currents (i_k in Eq.3) are strongly dependent on the amount of "oxide" on the Pt surface [57] which in turn is temperature dependent. Even though the oxide coverage is a pre-exponential term, it is a temperature dependent quantity.

As for activation energies, the Tafel slope obtained for the Pt_3Ni, Pt_3Co and "Pt-skin" bimetallic surfaces is almost the same as for pure Pt with values faces, (see Table 1). Inspection of Table 1 reveals two important differences between the Tafel slopes for the ORR in $HClO_4$ versus H_2SO_4 on all surfces: (i) while a single linear Tafel slope was obtained in H_2SO_4 [1], two Tafel slopes can be extrapolated in $HClO_4$. (ii) while in H_2SO_4 the Tafel plots are directly proportional to the temperature in $HClO_4$ the Tafel plots are inversely proportional to the temperature. Very recently, we found that if the oxide formation on Pt (hkl) is controlled rather with strongly adsorbing anions of supporting electrolytes (e.g. Br^-, HSO_4^-) than with temperature of electrolytes, then the i-E relationship has an ideally temperature-dependent Tafel slope (-2 x 2.3(RT/F) [50;55]. On the other hand, it was demonstrated that when temperature plays an important role in the oxide formation on Pt(hkl), e.g. as in alkaline solutions, then the $\partial \log i / \partial E$ relationship is inversely

[1] The number of data points in the "low current density" potential region is relatively small in H_2SO_4 and barely more than the minimum of three points to determine the slope.

proportional to the RT/F term [57]. Hence, in H_2SO_4 electrolyte the i-E relationship is in good agreement with a classical electrochemical kinetic theory [58] which predicts that the Tafel slope should be directly proportional to the temperature. In $HClO_4$, however, decreasing of the "apparent" Tafel slopes with increasing temperature on all electrodes may indicate that the $\partial \log i / \partial E$ contains a significant contribution from the temperature dependence of oxide formation on these electrodes as found for the ORR on Pt(hkl) in alkaline solutions [57].

3.4 Reaction pathway

The fact that essentially the same kinetic parameters are assessed from the analysis of experimental results for the ORR on all three surfaces implies that the reaction mechanism on Pt_3Ni and Pt_3Co alloy surfaces is the *same* as one proposed for pure Pt, *i.e.,* a "series" $4e^-$ reduction pathway which can be presented schematically as [50;55;59]:

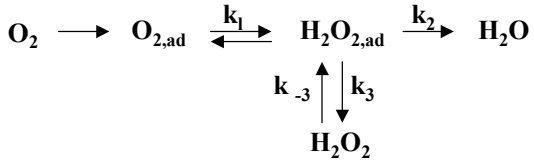

The first step in the overall reaction path is the adsorption of O_2 on the Pt surface,

$$O_2 \rightarrow O_{2(ad)} \qquad (4)$$

which is followed by the second rate determining step[2]

$$O_{2(ad)} + e^- \rightarrow O_2^-{}_{(ad)} \qquad (5)$$

If the rate controlling step is the first charge transfer step then, for the first order dependence of the kinetics of the ORR found in this work, the general rate expression is given by Eq (6).

$$i = nFKc_{O_2}(1-\Theta_{ad})^x \exp(-\beta FE/RT)\exp(-\gamma r\Theta_{ad})/RT) \qquad (6)$$

[2] It has been proposed that the rate determining step for the ORR on the Pt(111) surface in pure perchloric acid is also the first charge transfer step although the Tafel slope was different from 120 $mVdec^{-1}$ [50].

where n is the number of electrons, K is the rate constant, c_{O_2} is the concentration of O_2 in the solution, Θ_{ad} is the total surface coverage by adsorbed species (hydroxyl and bisulfate anions), x is the number of Pt sites occupied by the adsorbed ion, i is the observed current, E is the applied potential, β and γ are the symmetry factors (assumed to be ½), $r\Theta_{ad}$ is parameter characterizing the rate of change of the apparent standard free energy of adsorption with the surface coverage by adsorbing species, T is temperature, F is Faraday's constant and R is universal gas constant. A number of theories have been proposed to explain the transition in the Tafel slope on polycrystalline Pt electrode, i.e. to the change from Temkin to Langmuirian conditions for the adsorption of reaction intermediates [60-62], or as being due to a change in the surface coverage by OH_{ad} and specifically adsorbing anions which controls the availability the adsorption of molecular O_2 [46;47]. Very recently, based on Eq (4) it was developed a theoretical model which showed that in $HClO_4$ the best fit of the i-E relationship can be obtained by implying both blocking and energetic components [50]. In H_2SO_4, however, the energetic effect is of minor importance because the adsorption of reaction intermediates which are formed during the ORR occurs under Langmurian conditions [50;55]. Consequently, in H_2SO_4 the rate of the ORR may be correlated only with the availability of free Pt sites for the adsorption of reactants and intermediates, i.e. the $(1-\Theta_{ad})$ term. Closely following these arguments and based on the facts that Pt and Pt-alloys have the same Tafel slopes in both electrolytes one may suggest that in $HClO_4$ the Tafel slopes for the ORR on the Pt_3-Ni, Pt_3-Co and "Pt-skin" alloys are controlled by both energetic and blocking effects. In H_2SO_4, however, the rate of the ORR is predominantly determined by the surface coverage of bisulfate anions (blocking effects).

In previous studies [9-15], the principle explanation for the enhanced ORR activity on Pt-Ni and Pt-Co alloys was enumerated as being due one or more of the following effects: (i)

modification of the electronic structure of Pt (5-d orbital vacancies); (ii) change in the physical structure of Pt (Pt-Pt bond distance and coordination number); (iii) adsorption of oxygen containing species from the electrolyte onto the Pt or alloying element; and/or (iv) redox type processes involving the first row transition alloying elements.

Our results for the Pt_3Ni and Pt_3Co alloys suggest that, because the (chemical) rate constant K and the two exponential terms are essentially identical for all three systems, the ORR kinetics on these three surfaces is predominately controlled by the $(1 - \Theta_{ad})$ term. As discussed in ref. [5], in H_2SO_4 the $(1 - \Theta_{ad})$ term is mainly determined by the potential dependent specific adsorption of bisulfate anions. Figure 6 shows that at 0.8 V the catalytic effect of this term is a factor of 1.5. In $HClO_4$, however, the $(1 - \Theta_{ad})$ term is primarily determined with the potential dependent surface coverage of OH_{ad} species [50]. As one can see from Figure 5, the catalytic effect of this term is ca.1.5-2, consistent with the shift of ca. 50 mV in oxidation potential. We do not have a definitive explanation why Ni and Co in the Pt surface would cause either the decrease in the surface coverage by bisulfate anions or induce the positive shift in the oxidation potential of the Pt surface. In fact, a decrease in anion adsorption is just opposite what would one expect based on the change of the local potential of zero charge (pzc) of Pt atoms neighbored by Ni(Co). Notice that alloying Pt with less noble metals lowers the work function (pzc) of Pt surface and Pt atoms near the alloying elements (Ni,Co) have a positive charge with respect to Pt atoms far away [63], resulting in enhanced anion adsorption at these sites at a given electrode potential. The magnitude of the lowering of the pzc will depend on the state of the charge of alloying elements and other details of the Pt-Ni(Co) interaction, i.e., the local dipole moment. Although hypothetical, we offer some plausible explanation arguing that the local pzc concept might not be so important in controlling the adsorption of anions and oxide formation on the Pt-Ni(Co) surface. In particular, for specific adsorption of anions one may argue that the interaction of tetrahedral bisulfate anions is hindered

on alloy surfaces due to lack of ensemble of Pt atoms required for Pt-HSO_4^- interaction. Notice that Ni and Co are oxidized and therefore these sites are inactive for adsorption of bisulfate anions. In the case of Pt-OH, one may hypothesize that the adsorption of OH_{ad} *on* the Pt sites is modified due to mutual interaction between OH_{ad} and "oxide" covered Ni and Co atoms beyond 0.8 V. As for Pt-O interaction in UHV, the isosteric heat of adsorption of OH_{ad} on Pt sites (the surface coverage) surrounded by "oxide" covered Ni and Co atoms may significantly be reduced primarily from lateral repulsive interactions, and to much lesser extent the occupation of different adsorption sites. Therefore, being oxidized at much lower potentials then Pt, it appears that Ni and Co atoms may serve as "sacrificial" elements in Pt-Ni and Pt-Co alloys.

Figure 6 shows that, interestingly, the "Pt-skin" electrode has an uniquely high catalytic activity for the ORR in $HClO_4$. The rate of the ORR on the "Pt-skin" is increased by factor of 3-4 relative to a bulk Pt electrode. Very recently, a significant enhancement in the rate of the ORR in KOH was observed on pseudomorphic monolayer film of Pd [17] grown epitaxially on Pt(111). The monolayer film is about 5 times more active than Pd multilayer even though the latter is arougher surface. In this study it was proposed that the enhanced catalytic activity of the Pt(111)-Pd surface vs. the Pt(111) surface arise due to modification of surface electronic properties caused by charge redistribution upon forming the Pt-Pd bond. The same argument can be used for the "Pt-skin", e.g. due to the change of electronic structure the nature of oxide formation on the "Pt-skin" is changed causing the reduction of surface oxide to take place at more reversible potentials. Theoretical aspects of the relationships between the electronic structure and reactivity are, however, required in order to understand the trends in atomic/molecular chemisorption energies of oxygen containing species on the Pt_3Ni, Pt_3Co and "Pt-skin" bimetallic surfaces.

4. Conclussions:

The intrinsic catalytic activity of Pt_3Ni and Pt_3Co alloy catalysts for the ORR are studied on UHV prepared (annealing/sputtering cycles) and characterized (AES and LEIS) alloys in acid electrolytes. Polycrystalline bulk alloys of Pt_3Ni and Pt_3Co can be prepared in UHV having two different surface composition: one with 75 % Pt and the other with 100 % Pt. The latter we called a "Pt-skin" structure and is produced by an exchange of Pt and Co in the first layers. The base voltammetry in 0.1 M $HClO_4$ solution of the 75 Pt alloy surface indicated a decrease of H_{upd} pseudocapacitance (ca. 30-50 $\mu C/cm^2$) consistent with the surface composition determined by LEIS. Surprisingly, a decrease of H_{upd} pseudocapacitance was also observed on the "Pt-skin" electrode, consistent with the electronic effect of intermetalic bonding of the Ni(Co)-rich second layer with the top-most Pt atoms. Activities of Pt-alloys for the ORR were compared to the polycrystalline Pt in 0.5M H_2SO_4 and 0.1M $HClO_4$ electrolytes in the temperature range of $298 < T < 333$ K. With the exception of the "Pt-skin" surface on P_3Ni, all the alloy electrodes exhibited stable i-E curves with repeated cycling between 0.05-1.0 V at all temperatures. It was found that the order of activity is strongly dependent on the nature of anions of supporting electrolytes: in H_2SO_4 the activity increased in the order $Pt_3Ni > Pt_3Co > Pt$; in $HClO_4$, however, the order of activities at 333 K was "Pt-skin"$> Pt_3Co > Pt_3Ni > Pt$. The catalytic enhancement was greater in 0.1 M $HClO_4$ than in 0.5 M H_2SO_4, with the maximum enhancement observed for the "Pt-skin" on Pt_3Co in 0.1 M $HClO_4$ being 3-4 times that for pure Pt. Kinetic analyses of RRDE data revealed that kinetic parameters for the ORR and the production of H_2O_2 on the Pt_3Ni, Pt_3Co and "Pt-skin" alloys are the same as on pure Pt: the reaction order, m=1, two identical Tafel slopes in $HClO_4$ and a single Tafel slope in H_2SO_4, the "apparent" activation energy, ≈ 20-25 kJ/mol. The fact that essentially the same kinetic parameters are assessed from the analysis of experimental results for the ORR on all three surfaces implies that the reaction mechanism on

Pt_3Ni and Pt_3Co alloy surfaces is the *same* as the one proposed for pure Pt, *i.e.,* a "series" $4e^-$ reduction pathway. Catalytic enhancement of the ORR on Pt_3Ni and Pt_3Co vs. Pt was attributed to the inhibition of Pt-OH_{ad} formation *on* Pt sites surrounded by "oxide" covered Ni and Co atoms beyond 0.8 V.

Acknowledgment:

U.A. Paulus is greatly acknowledged for her contribution to some ORR measurements. This work was supported by the Assistant Secretary for Energy Efficiency and Renewable Energy, Office of Transportation Technologies Office of Advanced Automotive Technologies of the U.S. Department of Energy under contract No.DE-AC03-76SF00098.

Table 1: Kinetic parameters for the ORR on Pt and Pt bimetallic surfaces in a) 0.1M $HClO_4$ and b) 0.5M H_2SO_4

a)

Electrode	$\partial E/\partial \log(i_k)$ [mV/dec]		$\Delta H^{\#}$ [kJmol^{-1}] @η = 0.30V	m	n
	293K lcd/hcd	333K lcd/hcd			
Pt (pc)	81/112	67/87	21	1	4
Pt_3Ni-sputtered	86/113	54/78	23	1	4
Pt_3Co-sputtered	74/107	55/77	22	1	4
Pt_3Co-annealed	81/105	61/77	25	1	4

b)

Electrode	$\partial E/\partial \log(i_k)$ [mV/dec]		m	n
	293K	333K		
Pt (pc)	128	136	1	4
Pt_3Ni-sputtered	125	130	1	4
Pt_3Co-sputtered	118	131	1	4

$\partial E/\partial \log(i_k)$ – Tafel slope; **lcd/hcd**- low/high current density
$\Delta H^{\#}$ - Activation energy
m – Reaction order
n – Number of electrons

References:

1. Markovic, N. M.; Ross, P. N. *Surf.Sci.Reports* **2002**, *286*, 1-113.

2. EL Kadiri, F.; Faure, R.; Durand, R. *J.Electroanal.Chem.* **1991**, *301*, 177-188.

3. Markovic, N. M.; Gasteiger, H. A.; Ross, P. N. *J.Phys.Chem.* **1995**, *99*, 3411-3415.

4. Markovic, N. M.; Gasteiger, H. A.; Ross, P. N. *J.Phys.Chem.* **1996**, *100*, 6715-6721.

5. Markovic N. M.; Ross Jr., P. N. *Interfacial Electrochemistry - Theory, Experiments and Applications*; Marcal Dekker Inc.: New York, 1999; Chapter 46, pp. 821-841.

6. Climent, V.; Markovic, N. M.; Ross, P. N. *J.Phys.Chem.B* **2000**, *104*, 3116-3120.

7. Markovic, N. M.; Lucas, C.; Climent, V.; Stamenkovic, V.; Ross, P. N. *Surf.Sci.* **2000**, *465*, 103-114.

8. Appleby, A. J. *Catalysis Reviews* **1970**, *4*, 221-244.

9. Luczak, F. J. and Landsman, D. A. Ordered Ternary Fuel Cell Catalysts Containing Platinum, Cobal and Chromium. [US 4.447.506]. 1984.
   Ref Type: Patent

10. Lucas, C. A.; Markovic, N. M.; Ross, P. N. *Phys.Rev.B* **1997**, *55*, 7964-7971.

11. Luczak, F. J. and Landsman, D. A. Ordered Ternary Fuel Cell Catalysts Containing Platinum and Cobalt and Method for Making the Catalyst. [US 4.677.092]. 1987.
    Ref Type: Patent

12. Beard, B.; Ross Jr., P. N. *J.Electrochem.Soc.* **1990**, *137*, 3368.

13. Glass, J. T.; Cahen, G. L.; Stoner, G. E. *J.Electrochem.Soc.* **1987**, *134*, 58.

14. Mukerjee, S.; Srinivasan, S. *J.Electroanal.Chem.* **1993**, 201.

15. Toda, T.; Igarashi, H.; Uchida, H.; Watanabe, M. *J.Electrochem.Soc.* **1999**, *141*, 968.

16. Paulus, U. A.; Scherer, G. G.; Wokaun, A.; Schmidt, T. J.; Stamenkovic, V.; Radmilovic, V.; Markovic, N. M.; Ross, P. N. *J.Phys.Chem.B* **2001**, *106*, 4181-4191.

17. Markovic, N. M.; Schmidt, T. J.; Stamenkovic, V.; Ross, P. N. *Fuel Cells-from fundamentals to stems* **2001**, *2001*, 105-116.

18. Bardi, U.; Beard, B.; Ross, P. N. *J.Catal* **1990**, *124*, 22.

19. Ross Jr. P. N. *Electrocatalysis*; Wiley-VCH, Inc.: New York, 1998; Chapter 2, pp. 43-74.

20. Gasteiger, H. A.; Markovic, N.; Ross, P. N. *J.Phys.Chem.* **1995**, *99*, 16757-16767.

21. Gasteiger, H. A.; Markovic, N. M.; Ross Jr., P. N. *Catal.Let.* **1996**, *36*, 1-8.

22. Strohl, J. K.; King, T. S. *J.Catal* **1989**, *116*, 540.

23. Markovic, N. M.; Ross, P. N. *Electrochim.Acta* **2000**, *45*, 4101-4115.

24. Vasiliev, M. A. *J.Phys.D: Appl.Phys.* **1997**, *30*, 3037-3070.

25. Watson, P. R, Van Hove, M. A., and Herman, K. Atlas of surface stucture. [Volum IA, Monograph 5]. 1995. Washington,DC, ACS Publications.
Ref Type: Serial (Book,Monograph)

26. Gasteiger, H. A.; Markovic, N.; Ross, P. N.; Cairns, E. J. *J.Phys.Chem.* **1993**, *97*, 12020-12029.

27. Markovic, N. M.; Grgur, B. N.; Ross Jr., P. N. *J.Phys.Chem.B* **1997**, *101*, 5405-5413.

28. Sachtler, W. M. H.; van Santen, R. A. *Adv.Catal.* **1977**, *26*, 69.

29. Chelikowski, J. R. *Surf.Sci.* **1984**, *139*, L197.

30. Campbell, C. T. *Annu.Rev.Phys.Chem.* **1990**, *41*, 775-837.

31. Dowben, A. P.; Miller, A. *Surface segregation phenomena*, CRC Press: Boca Raton, 1990.

32. Polak, M.; Rubinovich, L. *Surface Science Reports* **1999**, *262*, 1-68.

33. Kuntze, J.; Speller, S.; Heiland, W.; Atrei, A.; Rovida, G.; Bardi, U. *Phys.Rev.B* **1999**, *60*, 1535-1538.

34. Kuntze, J.; Speller, S.; Heiland, W.; Deurinck, P.; Creemers, C.; Atrei, A.; Bardi, U. *Phys.Rev.B* **1999**, *60*, 9010-9018.

35. Niehus, H. *Phys.Status Solidi B* **1995**, *192*, 357.

36. Gauthier, Y.; Baudoing, R.; Rundgren, J. *Phys.Rev.B* **1985**, *31*, 6216-6218.

37. Bardi, U.; Atrei, A.; Zanazzi, E.; Rovida, G.; Ross Jr., P. N. *Vacuum* **1990**, *41*, 437-440.

38. Gauthier, Y. *Surf.Rev.and Letters* **2001**, *3*, 1663-1689.

39. Smith, D.P. *J.Appl.Phys.* **1967**, *38*, 340-347.

40. Taglauer, E. *Appl.Phys.A* **1985**, *38*, 161-170.

41. Paredes Olivera P.; Patrito, M. *Interfacial Electrochemistry, Theory, Experiment,and Applications*; Marcel Dekker, Inc.: New York, Basel, 1999; Chapter 5, pp. 63-81.

42. Clavilier, J. *J.Electroanal.Chem.* **1980**, *107*, 211-216.

43. Jerkiewicz, G. *Progress in Surface Science* **1998**, *57*, 137-186.

44. Markovic, N. M.; Schmidt, T. J.; Grgur, B. N.; Gasteiger, H. A.; Ross Jr., P. N.; Behm, R. J. *J.Phys.Chem.B* **1999**, *103*, 8568-8577.

45. Schmidt, T. J.; Paulus, U. A.; Gasteiger, H. A.; Alonso-Vante, N.; Behm, R. J. *J.Electrochem.Soc.* **1999**.

46. Tarasevich, M. R. *Electrochimiya* **1973**, *9*, 578.

47. Tarasevich, M. R.; Vilinskaya, V. S. *Electrochimiya* **1973**, *9*, 96.

48. Uribe, F.; Wilson, M. S.; Springer, T.; Gottesfeld, S. "Oxygen Reduction (ORR) at the Pt/Recast Ionomer Interface and Some General Comments on the ORR at Pt/Aqueous Electrolyte Interfaces".
Ref Type: Conference Proceeding

49. Adzic, R. R. "Surface Morphology Effects in Oxygen Electrochemistry"; Proceedings of the Workshop on Structural Effects in Electrocatalysis and Oxygen Electrochemistry.
Ref Type: Conference Proceeding

50. Markovic, N. M.; Gasteiger, H. A.; Grgur, B. N.; Ross, P. N. *J.Electroanal.Chem.* **1999**, *467*, 157-163.

51. Albery, W. J.; Hitchman, M. L. *Ring-Disc Electrodes*, Clarendon Press: Oxford, 1971.

52. 66th ed.; CRC Press: Boca Raton, FL, 1986.

53. Schumpe, A.; Adler, I.; Deckwer, W.-D. *Biotechnol.Bioeng.* **1978**, *20*, 145.

54. Anastasijevic, N. A.; Dimitrijevic, Z. M.; Adzic, R. R. *Electrochim.Acta* **1986**, *31*, 1125-1130.

55. Grgur, B. N.; Markovic, N. M.; Ross Jr., P. N. *Can.J.Chem.* **1997**, *75*, 1465-1471.

56. Damjanovic, A.; Sepa, D. B. *Electrochim.Acta* **1990**, *35*, 1157-1162.

57. Schmidt, T. J.; Stamenkovic, V.; Arenz, M.; Markovic, N. M.; Ross, P. N. *Electrochim.Acta* **2002**, *1*, 1.

58. Vetter, K. J. *Electrochemical Kinetics*, Academic Press: New York, 1967.

59. Stamenkovic, V.; Markovic, N. M.; Ross Jr., P. N. *J.Electroanal.Chem.* **2000**, *500*, 44-51.

60. Damjanovic, A.; Genshaw, M. A.; Bockris, J. O. M. *J.Phys.Chem.* **2001**, *45*, 4057.

61. Damjanovic A. *Modern Aspects of Electrochemistry*; Plenum Press: New York, 1969; Chapter 5, pp. 369-483.

62. Tarasevich M. R.; Sadkowski, A.; Yeager, E. *Comprehensive Treatise in Electrochemistry*; Plenum Press: New York, 1983; Chapter 6, pp. 301-398.

63. Markovic, N. M.; Ross, P. N. *J.Electroanal.Chem.* **1992**, *330* , 499-520.

Figure captions:

Figure 1. a) Auger electron spectroscopy of annealed and mildly sputtered Pt_3Ni. **b)** Low energy ion scattering spectra of the same two surfaces. Also shown is schematic picture of the "Pt-skin" electrode and the sputtered Pt_3Ni electrode. **c)** Cyclic voltammetry (50mV/s) of Pt and two Pt_3Ni surfaces at 295 K in 0.5 M H_2SO_4 (upper curves) and o.1 M $HClO_4$ (lower curves).

Figure 2. . a) Auger electron spectroscopy of annealed and mildly sputtered Pt_3Co. **b)** Low energy ion scattering spectra of the same two surfaces. Also shown is schematic picture of the "Pt-skin" electrode and the sputtered Pt_3Co electrode. **c)** Cyclic voltammetry (50mV/s) of Pt and two Pt_3Co surfaces at 295 K in 0.5 M H_2SO_4 (upper curves) and o.1 M $HClO_4$ (lower curves).

Figure 3. a) Disk (i_D) and ring (I_R) currents (anodic sweep direction) during the ORR on mildly sputtered Pt_3Co in 0.1 M $HClO_4$ at a sweep rate of 20 mV/s; Ring potential, E=1.15 V; Collection efficiency: N=0.2. **b)** Tafel plot at 1600 rpm. **c**) Levich plot at varies electrode potentials.

Figure 4. a) Disk (i_D) and ring (I_R) currents (anodic sweep direction) during the ORR on mildly sputtered Pt, Pt_3Co, and Pt_3Ni in 0.1 M $HClO_4$ at 293 K. **Insert b:** Tafel plots for all three surfaces at 293 K. **c)** Disk (i_D) and ring (I_R) currents (anodic sweep direction) during the ORR on mildly sputtered Pt, Pt_3Co, and Pt_3Ni in 0.1 M $HClO_4$ at 333 K. **Insert d:** Tafel plots for all three surfaces at 333 K. Sweep rate: 20 mV/s; Ring potential, E=1.15 V; Collection efficiency: N=0.2. **Insert e:** Arrhenious plots at overpotential of 0.3 V for the ORR on Pt, Pt_3Co, and Pt_3Ni electrodes.

Figure 5. a) Disk (i_D) and ring (I_R) currents (anodic sweep direction) during the ORR on mildly sputtered Pt, Pt_3Co, and Pt_3Ni in 0.5 M H_2SO_4 at 293 K. **Insert b:** Tafel plots for all three surfaces at 293 K. **c)** Disk (i_D) and ring (I_R) currents (anodic sweep direction) during the ORR on

mildly sputtered Pt, Pt_3Co, and Pt_3Ni in 0.5 M H_2SO_4 at 333 K. **Insert d:** Tafel plots for all three surfaces at 333 K. Sweep rate: 20 mV/s; Ring potential, E=1.15 V; Collection efficiency: N=0.2.

Figure 6. . a) Disk (i_D) and ring (I_R) currents (anodic sweep direction) during the ORR on UHV annealed Pt and Pt_3Co electrodes in 0.1 M $HClO_4$ at 293 K. **Insert b:** Tafel plots for these two surfaces at 293 K. **c)** Disk (i_D) and ring (I_R) currents (anodic sweep direction) during the ORR on UHV annealed Pt and Pt_3Co electrodes in 0.1 M $HClO_4$ at 333 K. **Insert d:** Tafel plots these two surfaces at 333 K. Sweep rate: 20 mV/s; Ring potential, E=1.15 V; Collection efficiency: N=0.2. **Insert e:** Histograms showing the kinetic currents densities at E= 0.85 V for the catalysts in this study obtained at 333 K.

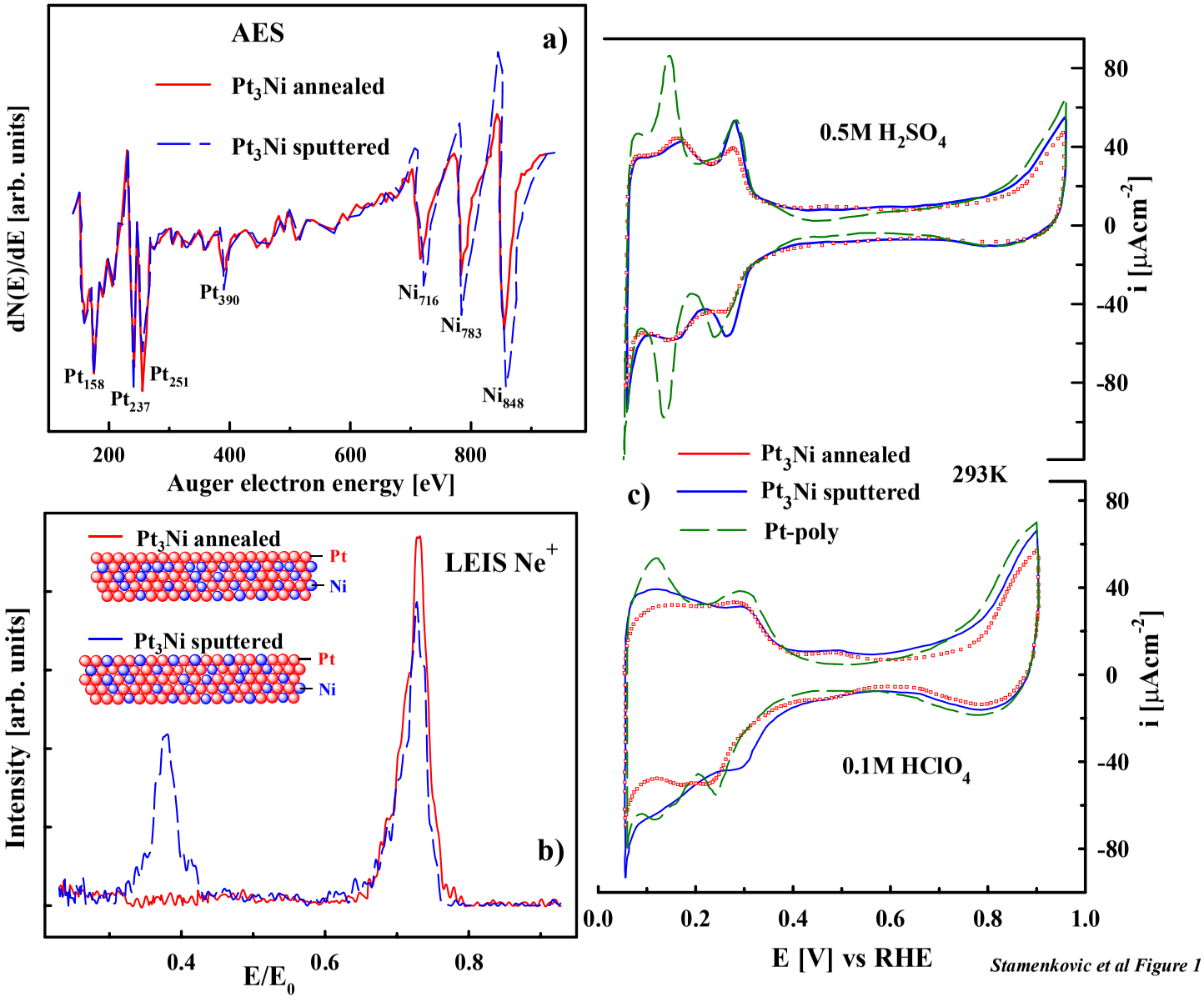

Stamenkovic et al Figure 1

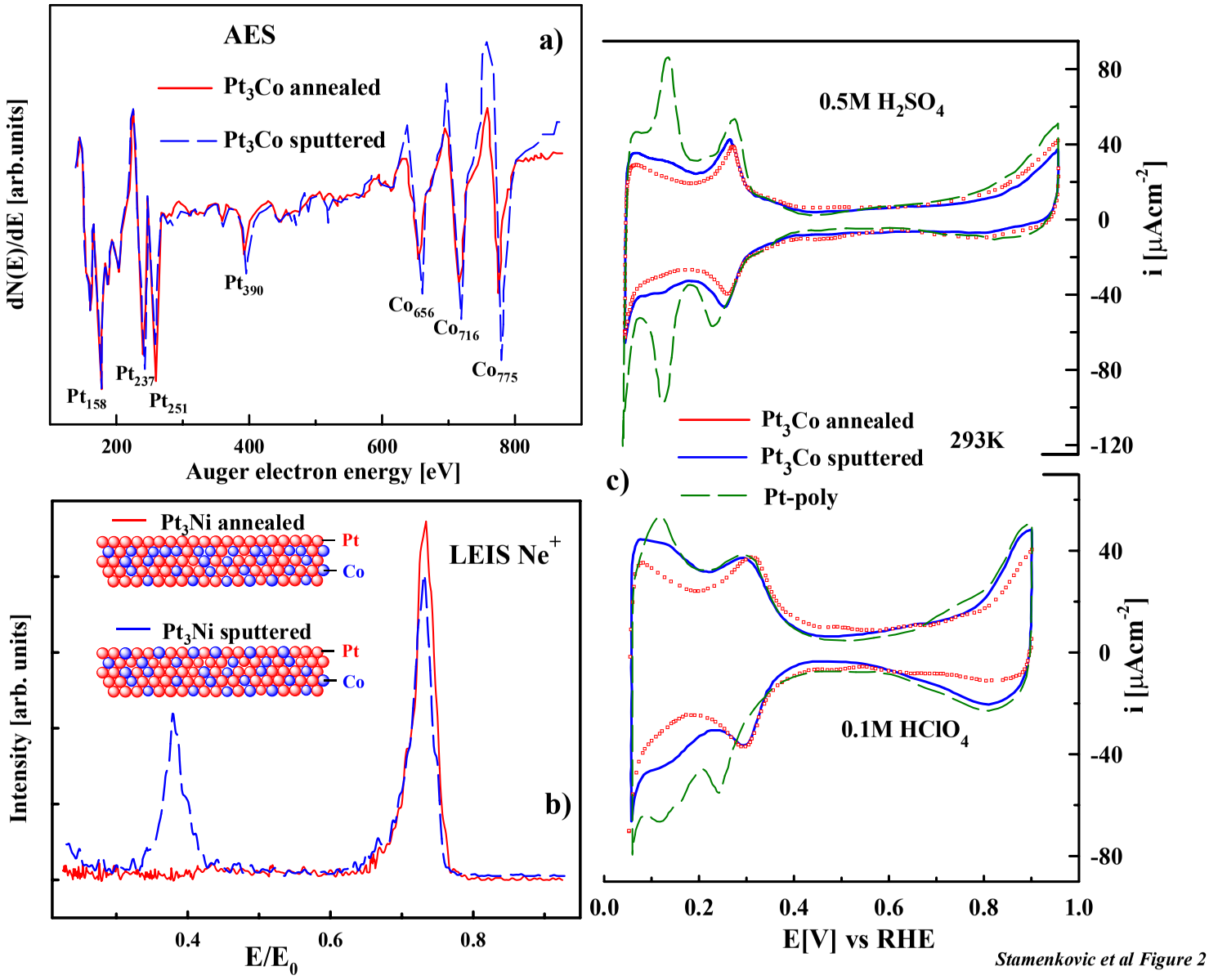

Stamenkovic et al Figure 2

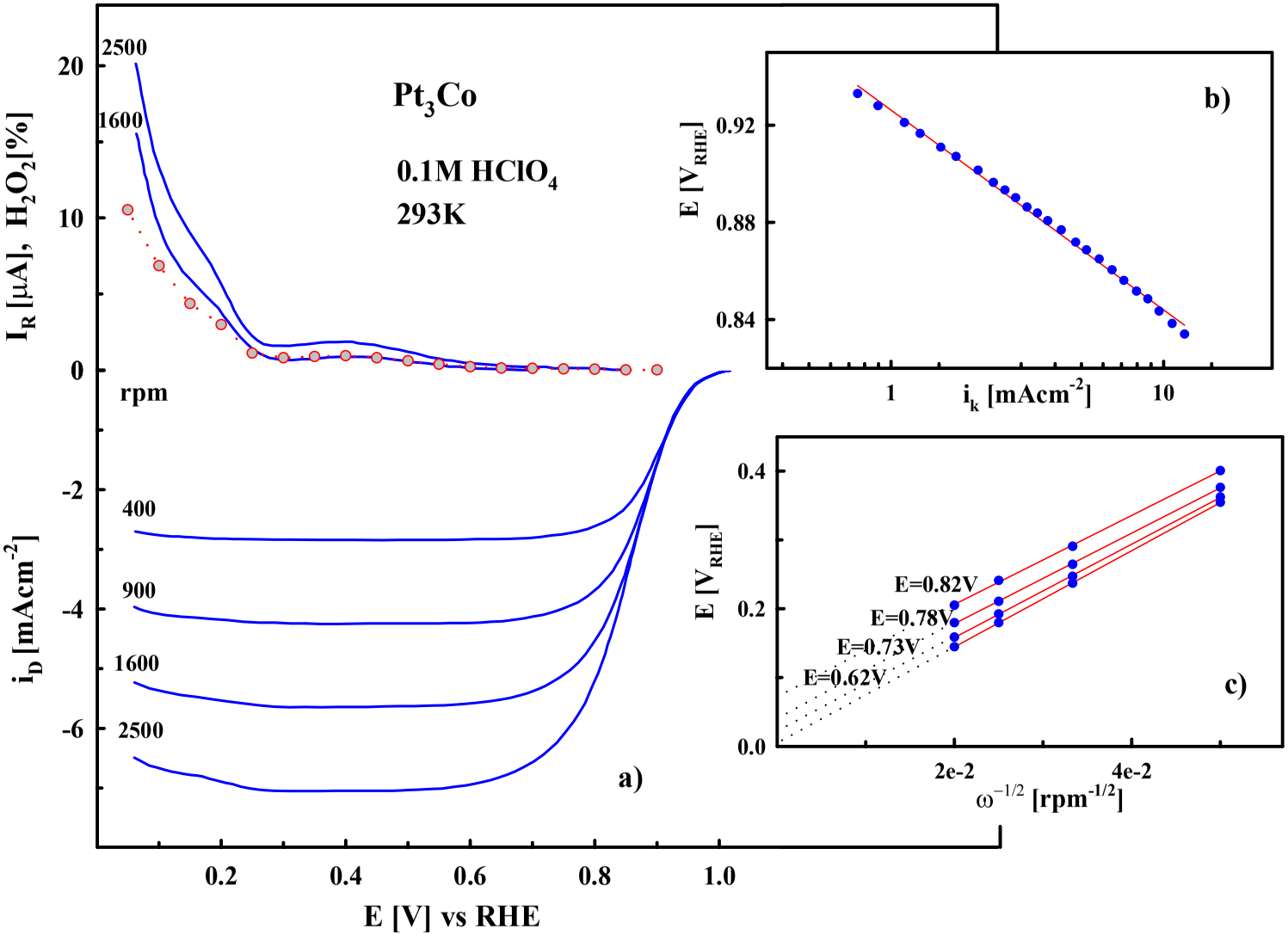

Stamenkovic et al., Figure 3

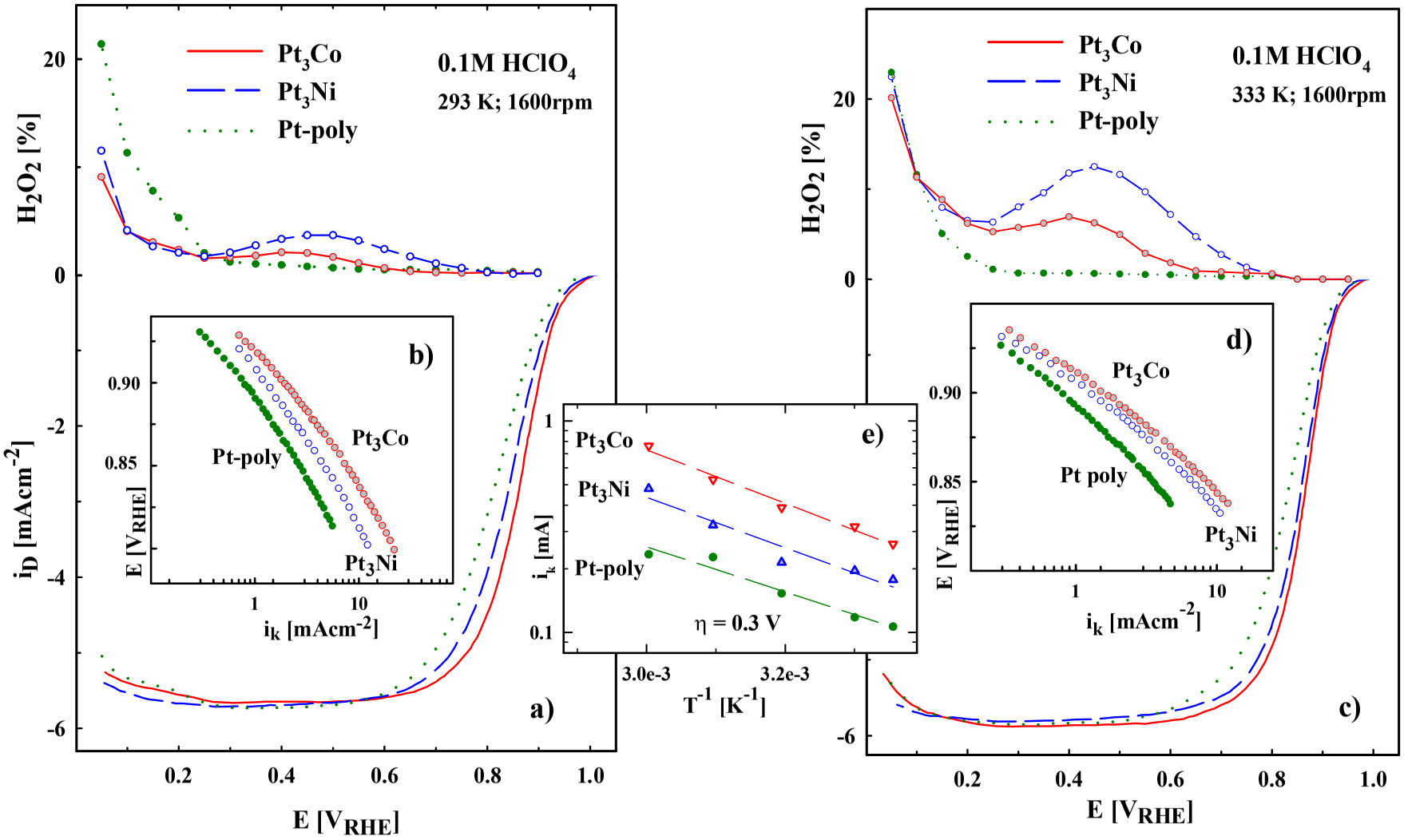

Stamenkovic et al., Figure 4

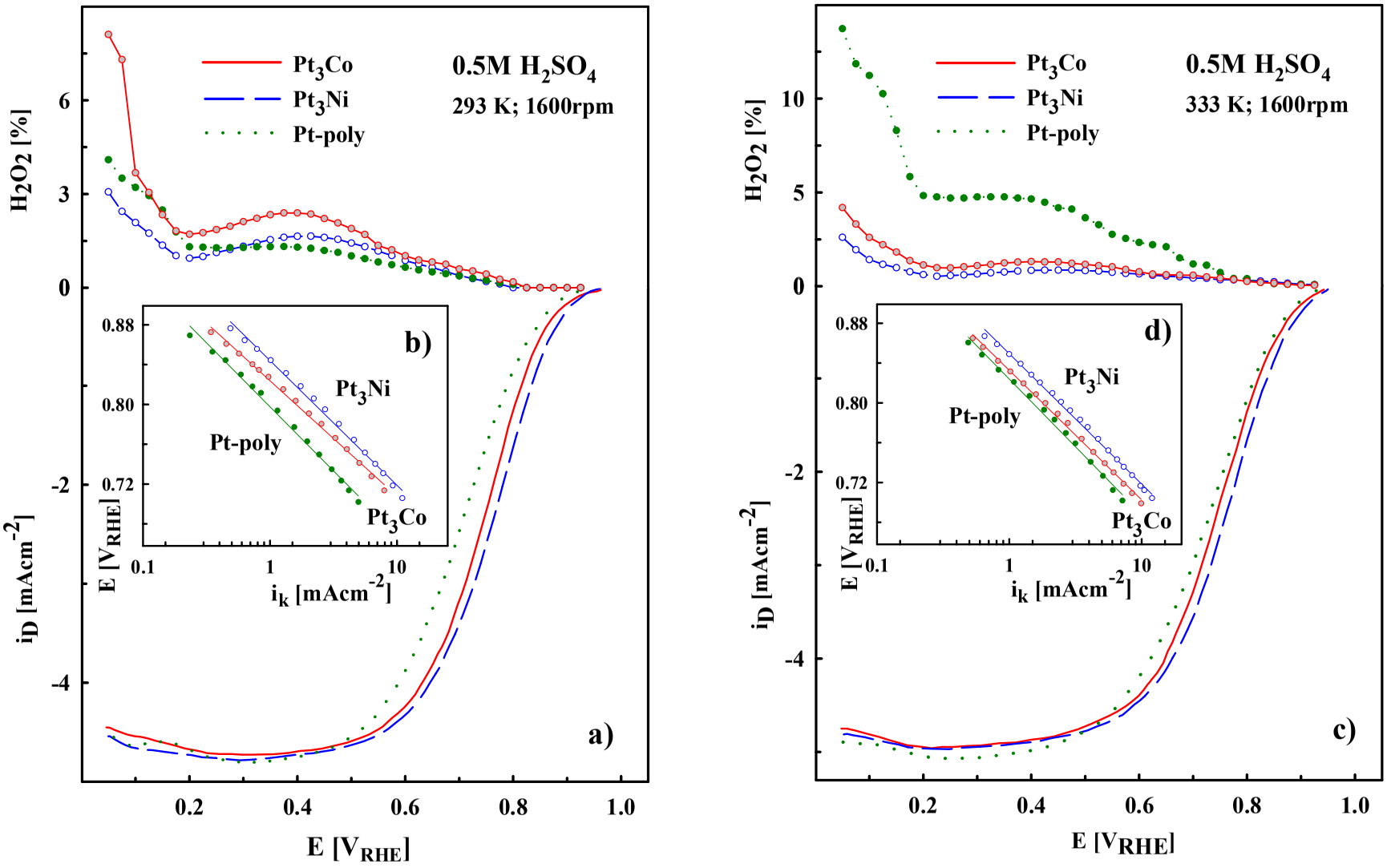

Stamenkovic et al., Figure 5

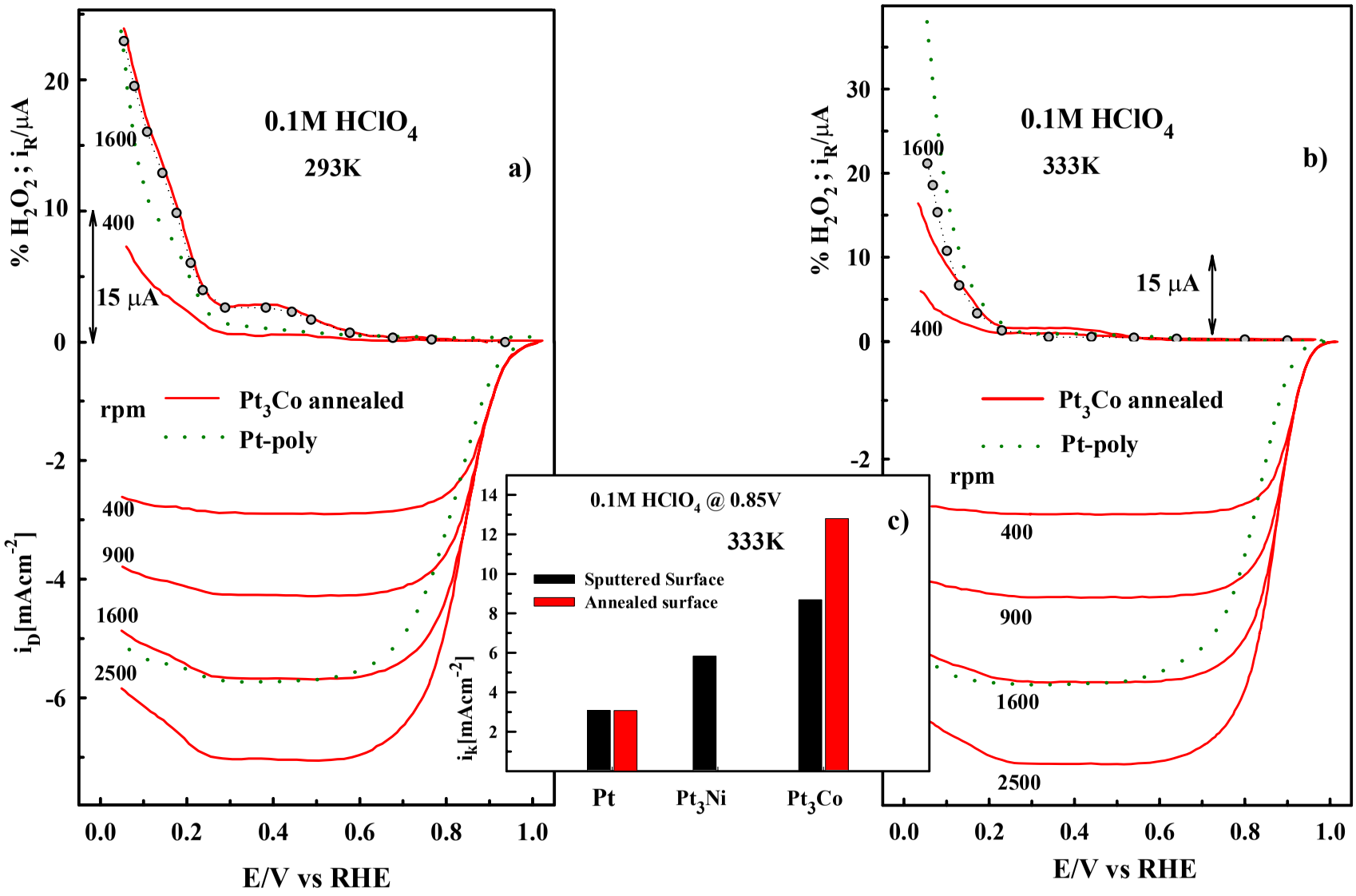

Stamenkovic et al Fig. 6